Adsorption of Cadmium by Magnesium-modified Biochar at Different Pyrolysis Temperatures

Ya Chen, Ruifeng Shan,* and Xiaoyin Sun

Metal pollution in soil is an increasing concern. Cadmium poses significant risks to ecosystems, and methodologies for its removal, including adsorption, have been researched. There are several environmentally friendly adsorbing materials (such as Biochar) for Cd removal. In this study, to improve the adsorptive capacity of Cd, coconut and peanut shells were used as raw materials to prepare Biochar at 300 °C and 600 °C. The effects of the pyrolysis temperature and material type on the physicochemical properties of the adsorbents were investigated by elemental analysis, scanning electron microscopy, and Fourier transform infrared spectroscopy. Magnesium-loaded BC was synthesized to determine its Cd^{2+} absorptivity. The adsorption characteristics and mechanisms of Cd^{2+} in an aqueous phase were studied through batch adsorption experiments. The results demonstrated that the pseudo-second-order kinetics model accurately described the adsorption kinetics of adsorbents of Cd^{2+}. The adsorption behavior of the Cd^{2+} adsorbent conforms to the single layer adsorption described by the Langmuir model. Adsorption of Cd^{2+} involves a spontaneous endothermic process. The initial pH of the solution greatly influenced the adsorption of Cd^{2+} and showed a trend of rapid growth and then slow growth. Thus, magnesium-modified biomass carbon has good potential for applications in pollutant remediation.

Keywords: Cd adsorption; Modified BC; Mg doping; Adsorption mechanism

*Contact information: College of Geography and Tourism, Qufu Normal University, Rizhao, 276826, P. R. China; *Corresponding author: ruifengshan@sina.com*

INTRODUCTION

Soil heavy metal pollution is a common environmental issue. Cadmium （Cd^{2+}） is one of the most toxic heavy metals, causes great harm to human health, and is a serious threat to the surrounding environment. The concentration of Cd^{2+} in mining, smelting, and sewage irrigation areas in China is significantly higher than in remote areas. In spatial distribution, the content of Cd^{2+} in southern areas is higher than in northern areas. The content of Cd^{2+} in soils is 0.27 $mg \cdot kg^{-1}$ in southern areas, which exceeds the national first-level soil environmental quality standard (Luo. 2018). In April 2014, the Ministry of Environmental Protection and the Ministry of Land and Resources of China announced the state of soil pollution in the entire country. The results demonstrated that cadmium was the main soil pollutant in soil of China.

Biochar (BC) is one of the many soil amendments. Because of its special structure and property, such as huge specific surface area, its richness in oxygen-containing functional groups, and a large number of surface charges, BC could be an alternative absorbent. In recent years, BC has been widely used in the repair of soils contaminated by heavy metals.

Recent studies have encouraged the production and optimization of adsorbent

materials that have characteristics similar to that of activated carbon (C) materials but are cost efficient and environmentally friendly (Inyang *et al*. 2010). For example, BC is a pyrogenic carbon material produced by thermal conversion of lignocellulose biomass under oxygen-free or limited conditions (Lehmann *et al*. 2006; Song *et al*. 2014). Because of its unique properties such as high surface area and cation exchange capacity, BC can be used for soil improvement, fertility enhancement, and carbon sequestration applications (Zimmerman *et al*. 2011; Mohana *et al*. 2014). However, the ability of BC to remove contaminants from aqueous solutions is limited (Yao *et al*. 2013). Improvements are reflected in the large number of engineered BCs with novel structures and surface properties (Zhang *et al*. 2013; Song *et al*. 2014). Studies have focused on the synthesis of carbon-based binary metal oxide composites for removing heavy metals from aqueous solutions (Tang *et al*. 2014).

Copper (Cu^{2+}) and Cd^{2+} have been successfully removed from aqueous solution by adsorption by ferromanganese binary oxide–BC composites prepared through impregnation/sintering methods. The process is accurately represented by the Freundlich and Langmuir models and is driven by spontaneous endothermic entropy reduction (Zhou *et al*. 2018; Wang *et al*. 2015). Coconut shell BC, is mixed and wrapped with impurities during its production process, which reduces its original microstructure characteristics and remediation efficiency (Jia *et al*. 2016; Paranavithana *et al*. 2016). Acid pickling and ultrasonic treatment methods improve the physicochemical properties of BCs, the immobilization effect of heavy metals, and the soil micro-environment. The acid-soluble Cd, Nickel (Ni), and Zinc (Zn) elements were decreased by 30.1%, 57.2%, and 12.7%, respectively (Liu *et al*. 2018a). Therefore, it is necessary to modify the microstructure and surface properties of BC to enhance its remediation ability (Rajapaksha *et al*. 2016; Fang *et al*. 2018). Magnesium-modified biochar (MBC) is a kind of new material that can load magnesium oxide on the surface of BC (Zhou *et al.* 2012). It can be made from agricultural straw, garden waste, municipal sludge, and other biomass wastes (Fang *et al*. 2015). Moreover, the pyrolysis conditions, such as the solubility of the impregnated solution and the pyrolysis temperature, affect the surface properties of the BC, thus affecting its adsorption properties for inorganic and organic compounds (Novais *et al*. 2018). The adsorbed MgO modified BC can be used in agricultural slow-released fertilizer to supplement phosphorus and potassium and improve soil nutrition. Meanwhile, due to its rich fixed carbon, it can improve the carbon content in the soil and improve the physical and chemical properties of the soil (Beesley *et al.* 2011). Therefore, the use of biomass materials such as waste to prepare MBC to repair heavy metals in the soil can improve soil conditions, and can also realize waste resource treatment, providing a more ecological and green solution for waste treatment. However, the effectiveness of magnesium-modified and ultrasonic-modified BC and their implications for contaminated soil remediation processes have not been systematically studied. Therefore, magnesium modification and ultrasonic treatment were chosen to enhance the physical and chemical properties of BC, as well as the immobilization effect of heavy metals and water micro-environment.

The objectives of this study were (1) to prepare and characterize BC and MBC composites; (2) to analyze the adsorption properties of MBC in an aqueous solution; and (3) to define the mechanisms involved in the adsorption of Cd^{2+} by MBC.

EXPERIMENTAL

BC Preparation

The coconut shell was produced in Hainan, and the peanut shell was produced in Shandong, China. The coconut and peanut shells were washed with deionized water, dried and pulverized, passed through a 10-mesh sieve. The coconut shell biomass and peanut shell biomass were then placed into a porcelain crucible and capped, were pyrolyzed at desired temperature (300 or 600 °C) under N_2 environment at the rate of 10 °C min^{-1}, and then kept for 2 h at that temperature (Sun *et al*. 2017). After cooling to room temperature (25 °C), the BC was ground and sieved through a 0.6 mm sieve and washed with deionized water for a few times, then dried at 70 °C for 6 h, and finally put in a closed container before use.

0.1 M $MgCl_2$ solution was prepared to modify the BC. A certain amount of the coconut shell BC and peanut shell BC were immersed in the $MgCl_2$ solution (solid/liquid ratio was fixed at 1:10), soaked in an ultrasonic oscillator for 6 h, filtered, cleaned, placed in a crucible, and oven-dried at 105 ℃. The samples were placed in a resistance furnace control box and carbonized at 300 ℃ for 2 h (without protecting gas), then cooled to room temperature to obtain a modified coconut shell charcoal and modified peanut shell, respectively. The original BC samples were designated "BC" and the modified BC samples were designated "MBC" with a suffix indicating the peak temperature of pyrolysis: coconut shell pyrolyzed at 300 ℃ (300 YBC); coconut shell pyrolyzed at 600 ℃ (600 YBC); peanut shell pyrolyzed at 300 ℃ (300 HBC); poultry manure pyrolyzed at 600 ℃ (600 HBC); coconut shell pyrolyzed at 300 ℃ and doped with $MgCl_2$ (300 MYBC); coconut shell pyrolyzed at 600 ℃ and doped with $MgCl_2$ (600 MYBC); peanut shell pyrolyzed at 300 ℃ and doped with $MgCl_2$ (300 MHBC); and peanut shell pyrolyzed at 600 ℃ and doped with $MgCl_2$ (600 MHBC).

Sorbent Characterization

The surface morphology of the samples was characterized using by scanning electron microscopy (SEM) (Hitachi S-4800, Tokyo, Japan). The surface functional groups were determined via Fourier transform infrared spectroscopy (FTIR) (Bruker TENSOR 27, Karlsruhe, Germany). Brunauer–Emmett–Teller (BET) specific area, porosity and pore size distribution were characterized by a porosimetry analyzer (AUTO-SORBiQ2, Quantachrome, USA).The elemental composition of BC was determined with an elemental analyzer (Vario EL III, Elementar, Berlin, Germany). The crystallographic structure of the samples was examined through X-ray diffraction (XRD) analysis (Ultima IV, Japan).

Adsorption Experiments

All adsorption experiments were conducted in 100 mL conical glass bottles. The bottles were placed in a thermostatic rotary shaker with a speed of 200 rpm for 24 h at 25 ± 1 °C. All sorption studies were conducted in triplicates, and the average values were used for the data analysis.

For the adsorption kinetic studies, 0.05 g of the prepared samples were added to a Cd^{2+} solution (25 mL, 100 $mg \cdot L^{-1}$) and stirred at 200 rpm. Aliquots (0.5 mL) were sampled at different time intervals (5, 10, 15, 30, 60, 120, 300, 600, 720, and 1440 min), filtered through a 0.45-μm filter, and analyzed by atomic absorption spectrophotometer (AAS). The following pseudo-first-order, pseudo-second-order kinetic, and intra-particle

diffusion equations were used to fit the data (Chen *et al*. 2018a),

pseudo-first-order equation: $q_t = q_e(1 - e^{-k_1 x})$ (1)

pseudo-second-order equation: $\frac{t}{q_t} = \frac{k_2 q_e^2 t}{1+k_2 q_e^t}$ (2)

Intra-particle diffusion equation: $q_t = K_{pi} t^{0.5} + C_i$ (3)

where q_t is the adsorption amount at the time, (mg·g^{-1}); K_1 is the pseudo-first- order kinetic constant, (min^{-1}); K_2 is the pseudo-second-order adsorption rate constant, (g·mg^{-1}·min^{-1}); K_p is the intra-particle diffusion constant, (mg·g^{-1}·min$^{-1/2}$); t is the adsorption time, (min); and C is the intercept, which indicates the size of the boundary reaction, assuming that q_t and $t^{1/2}$ are linear. At the coordinates (0,0) of the coordinate curve, the adsorption reaction belongs to the intra-particle diffusion.

The isotherm was recorded at the initial Cd^{2+} concentrations of 20.0, 40.0, 80.0, 120.0, 160.0, and 200.0 mg·L^{-1} at 25/35 and 45 °C. 0.05 g of the prepared samples were added to a Cd^{2+} solution and stirred at 200 rpm then filtered through a 0.45-μm filter, and analyzed by AAS. The dosage of the samples was 25 mL, and the solution pH was 6.03. The following Langmuir and Freundlich equations were used to fit the data and study the equilibrium adsorption behavior of MgBC,

Langmuir equation: $q_e = \frac{q_m C_e}{K_L + C_e}$ (4)

Freundlich equation: $q_e = K_F + C_e^n$ (5)

where K_L represents the interaction energy (mg·L^{-1}), K_F represents coefficient of affinity; q_m is the theoretical adsorption saturation, (mg·g^{-1}); q_e is the maximum adsorption capacity (mg·g^{-1}); C_e is the concentration of Cd^{2+} in the equilibrium solution (mg·L^{-1}), and n is linearity constant.

To test the pH effect, the solution was adjusted to a constant pH of 3, 4, 5, 6, 7, and 8. 0.05 g·L^{-1} of all adsorbents was mixed with 25 mL of the 100 mg·L^{-1} Cd^{2+} solution and stirred at 200 rpm then filtered through a 0.45-μm filter, and analyzed by AAS.

Statistical Analysis

The experimental data were analyzed and plotted with Excel 2010 and Origin 8.0.

RESULTS AND DISCUSSION

Sorbent Properties

The pore structure of BC has a great influence on the physical adsorption process. Different pore structures engender an inconsistent transport and diffusion rate of Cd^{2+} in BC. The stability of Cd^{2+} adsorbed by BC is low. Thus, Cd^{2+} is easily rereleased when the conditions change (Ahmad *et al.* 2013). The structure of the BC material is changed by modifications. The analysis of the parameters of the specific surface area, total pore volume, and average pore size are shown in Table 1. The order of the specific surface area of BC was 300 MYBC > 600 MYBC > 300 YBC > 600 YBC; 300 MHBC > 600 MHBC > 300 HBC > 600 HBC. After Mg modification, the specific surface area and pore volume of raw carbon increased, but the average void width decreased compared with the raw carbon. These results demonstrate that oxidation of $MgCl_2$ expands the specific surface area and pore volume of raw carbon.

Table 1. Pore Structure of the Carbon Materials

BC	300 YBC	600 YBC	300 HBC	600 HBC	300 MYBC	600 MYBC	300 MHBC	600 MHBC
BET specific surface area ($m^2 \cdot g^{-1}$)	3.04	1.77	25.60	34.00	67.96	79.95	147.47	184.71
Total pore volume ($cc \cdot g^{-1}$)	0.01	0.01	0.15	0.05	0.051	0.02	0.084	0.09
BET specific surface area (D^-/nm)	4.72	1.19	1.18	4.16	2.12	1.62	1.18	1.18

The main factors affecting the adsorption performance of BC are the specific surface area and pore volume (Cui *et al.* 2010). Generally, the larger the specific surface area and pore volume, the stronger the adsorption performance of BC. Figure 1 shows the nitrogen adsorption-desorption curves of coconut shell and peanut shell BC samples.

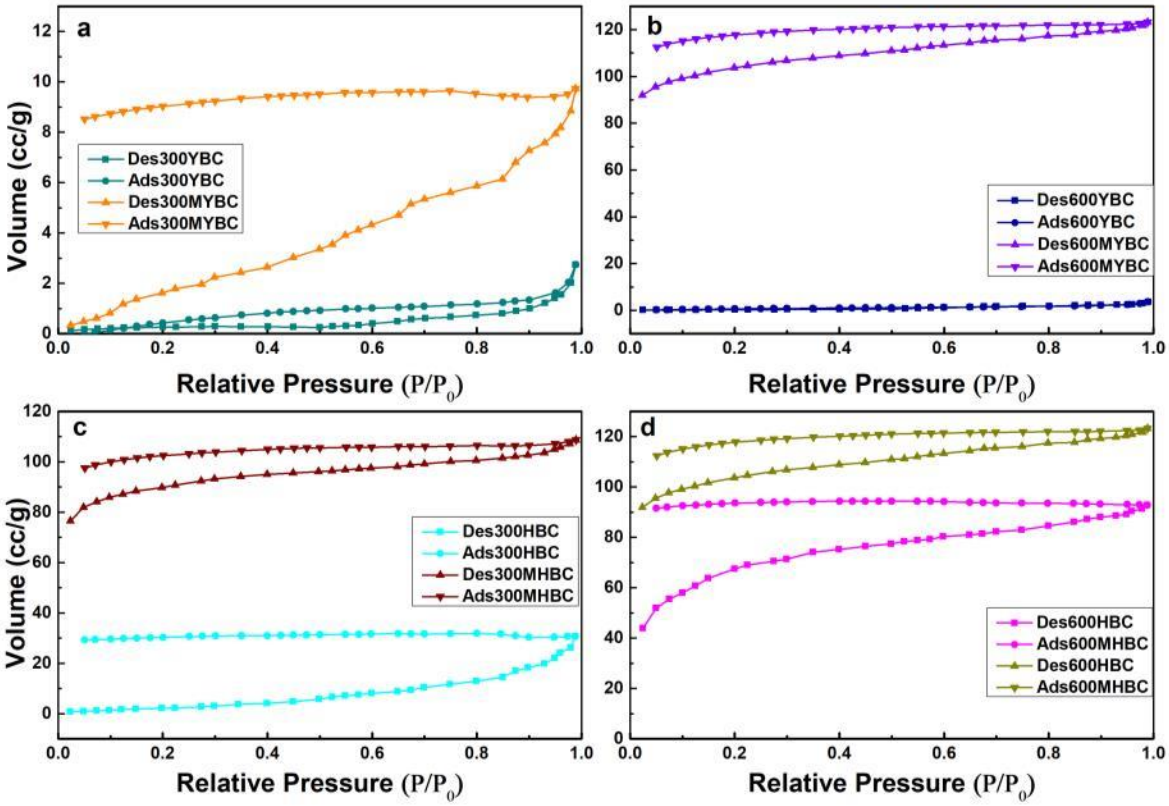

Fig. 1. The nitrogen adsorption-desorption curves of BC and MBC at different temperatures: (a) 300YBC and 300MYBC (b) 600YBC and 600MYBC (c) 300HBC and 300MHBC (d) 600HBC and 600MHBC

It can be seen from Fig. 1 that when $P / P_0 = 1$, the nitrogen adsorption capacity increased at 300 ~ 600 ℃, indicating that the pore structure of the material developed gradually and the total pore volume increased with the increase of pyrolysis temperature in this stage. The adsorption isotherms of coconut shell at 300 ℃ and 600 ℃ showed obvious adsorption platforms. According to the six types of adsorption isotherms defined

by IUPAC (Xu *et al.* 2015), the isotherms are typical T-type, namely microporous type. The adsorption isotherms of peanuts shell BC are all in inverse S shape. When the relative adsorption pressure was low (P / P_0 < 0.2), the adsorption capacity of the sample at 300 ℃ declined. At this time, there is an inflection point, indicating that the pore completes the monolayer adsorption, and then with the increase of the relative adsorption pressure, the adsorption capacity of nitrogen increased slightly, but the increased amplitude of capacity was small, and so the curve tended to be horizontal. When the relative adsorption pressure is low, the adsorption capacity of nitrogen slightly increases. When the pressure was high (P / P_0 > 0.8), the nitrogen adsorption capacity of the samples increased, which indicated that the pore structure of BC was mainly mesopores and macropores (Liu *et al.* 2005), and the adsorption capacity of magnesium modified BC and 600 ℃ peanut shell samples in the low pressure zone increased rapidly. It reflects the existence of micropores in the BC material at this time. When the pressure was close to saturation, the adsorption capacity of nitrogen increased. It is also obvious that the reason may be the capillary condensation phenomenon similar to the macropore. This is similar to the conclusion following from pore size analysis.

The functional groups of BC affect its chemisorption. There are multiple functional groups such as carboxyl, hydroxyl, and amino groups on the surface of carbon materials. A higher number of oxygen-functional groups results in stronger cation exchange ability and stronger adsorptive capacity of Cd^{2+} (Ahmad *et al*. 2013). Figure 2 (a) shows that the functional groups of magnesium-modified BC (300 MYBC, 600 MYBC) were similar to those of coconut shell BC (300 YBC, 600 YBC). The broad peak of coconut shell BC was observed at 3423 cm^{-1}, which corresponds to the stretching vibration of hydroxyl (-OH). The peak at 2922 cm^{-1} corresponds to the stretching of the C-H bonds of methyl and methylene. The peak at 1567 cm^{-1} represents the antisymmetric stretching of -COO (Yuan *et al*. 2011). The peak at 1014 cm^{-1} is attributed to the stretching vibration of the alcohol group and C-OH of the carboxylic acid. In addition, the polarization vibration and symmetrical stretching of carboxylate (-COO) are observed at 776 cm^{-1}. The absorption peak of coconut shell BC decreased when the temperature rose to 600 ℃.

As observed in Fig. 2 (b), peanut shell BC showed obvious absorption peaks at 3462, 2944, 1633, 1450, 1009, and 833 cm^{-1}, indicating that it contained abundant functional groups, but the surface functional groups of pyrolysis BC at different temperatures were different. When the pyrolysis temperature was increased from 300 ℃ to 600 ℃, the stretching vibration of -OH near 3462 cm^{-1} almost disappeared, indicating that the increase in pyrolysis temperature decreased the number of hydroxyl radicals, which may be due to the separation of bound water and the breakage of hydrogen bonded hydroxyl radicals (Jian *et al*. 2016). With the increased pyrolysis temperature, the aliphatic C-H (2944 cm^{-1}) decreased gradually, while the aromatic C-H (833 cm^{-1}) increased. This result indicates that the alkyl group of the peanut shell disappears gradually during the pyrolysis and the aromatization degree of BC increases gradually (Marco *et al*. 2010).

The infrared spectrum analysis showed that the characteristic peaks of MgO modified BC were similar to those of unmodified BC, indicating that MgO particles have little effect on the types of organic functional groups in BC (Fang *et al*. 2014; Takaya *et al*. 2016).

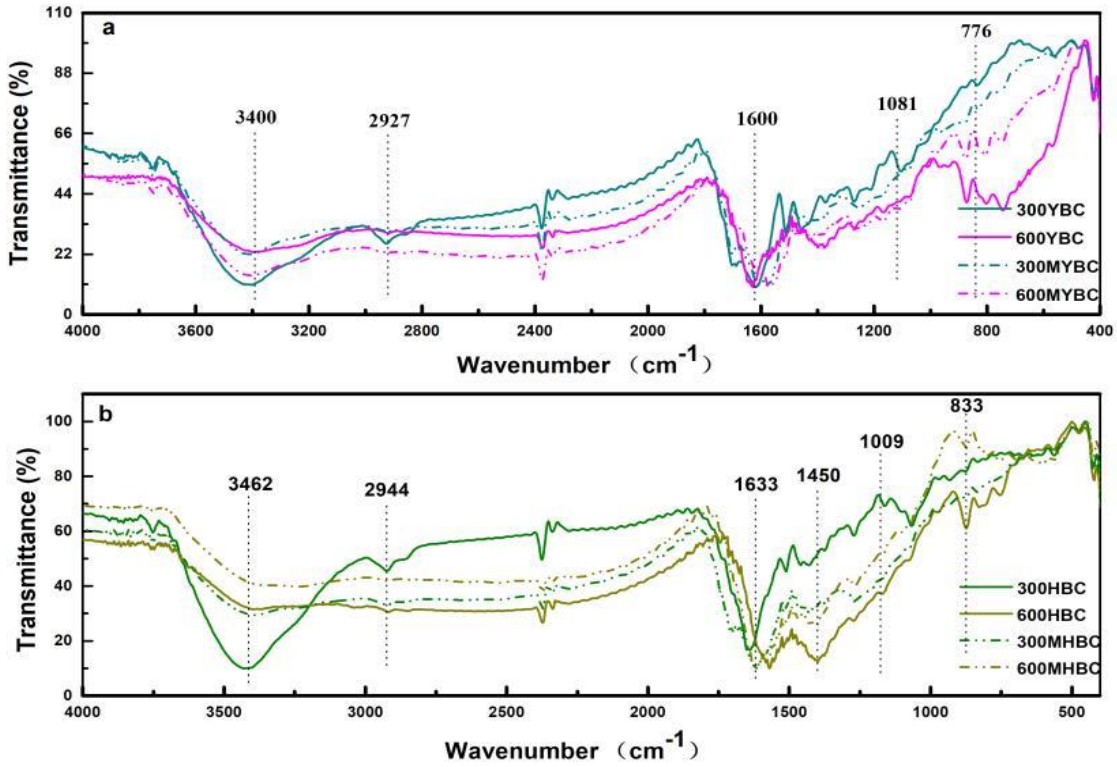

Fig. 2. Infrared spectra of BC and modified BC at different temperatures: (a) YBC and MYBC and (b) HBC and MHBC

As shown in Fig. S1 (a, b) of the Supplementary material, the surface of coconut shell BC presented multiple pores with different-sizes. On the pore walls of large holes, smaller holes were observed, and the pore walls show a network structure. In Fig. S2 (a, b) of the Supplementary material, the cross-section of the peanut shell BC presented an irregular columnar or massive surface, and a large number of pores, resulting in a large specific surface area, facilitating the adsorption of heavy metal pollutants. As shown in Supplementary material Fig. S1 (c, d) and Fig. 3 (c, d), a large number of cubic crystal particles appeared on the surface of modified BC. From the Energy Dispersive Spectrometer (EDS) test results in Fig. 3, the modified BC presented a Mg peak and the O peak increased. The white particles on the surface of the modified BC are magnesium oxides or hydroxyl compounds. These particles are MgO crystals (Jung *et al.* 2015b). The medium crystalline particles of 600 MYBC and 600 MHBC were evenly distributed compared to 300 MYBC and 300 MHBC.

Figure 4 shows the XRD wide angle diffraction patterns of YBC, MgO-YBC, HBC and MgO-HBC. The comparisons of the two samples modified by magnesium to the unmodified samples are shown in Fig. 4a and 4b, respectively. There is an obvious diffraction peak at 2 θ = 42.7 °. It has been shown that the peak should be the characteristic peak of MgO, which indicates that magnesium ions have been loaded on BC (Meng *et al.* 2017; Yang *et al.* 2018). Therefore, MgO was the most important crystal phase in the modified BC particles. Meanwhile, the related research also shows that when $MgCl_2$ is used as the modifier, the existing form of magnesium in the modified BC is MgO.

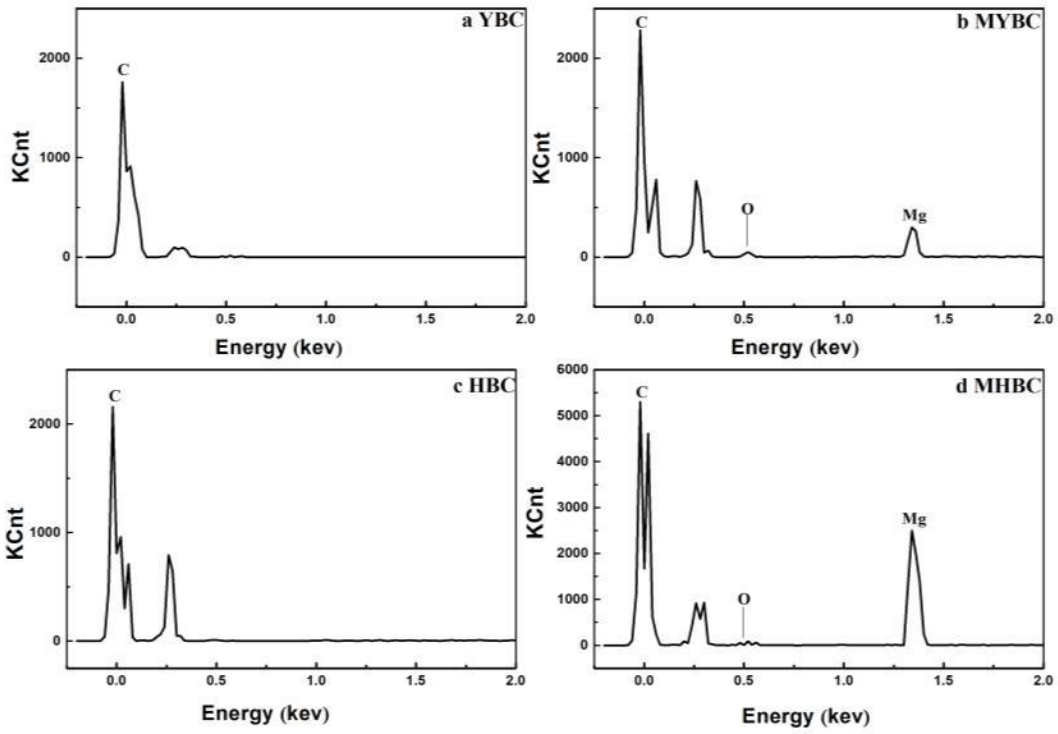

Fig. 3. Energy spectrum analysis charts of different types of BC

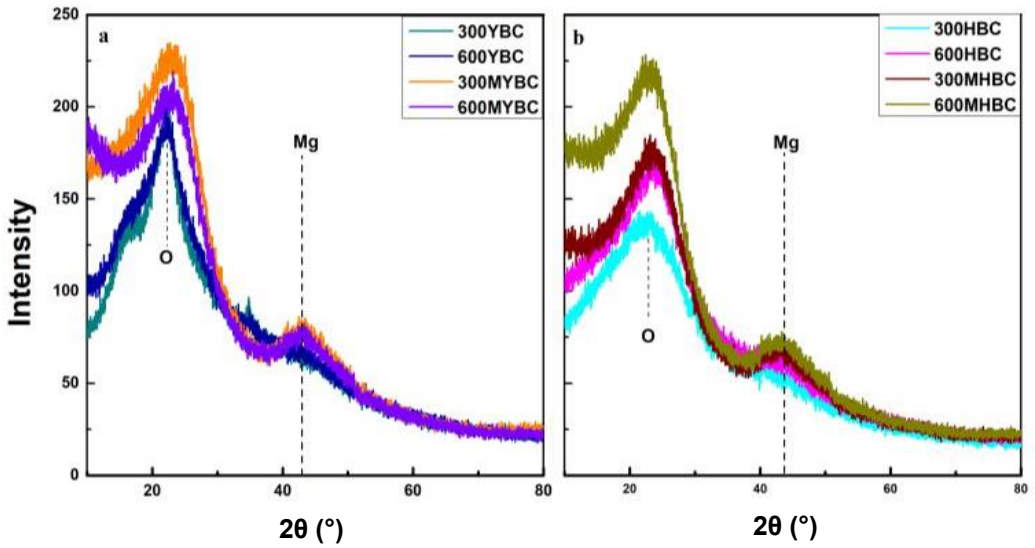

Fig. 4. XRD analysis charts of different types of BC

BC Adsorption Behavior for Cd^{2+}

Adsorption kinetics

Figure 5 shows the adsorption curve of BC and modified BC for Cd^{2+} at different adsorption times (the reaction contact time was controlled for 0 to 24 h). The adsorption capacity increased rapidly at the initial stage of adsorption, and then it gradually reached equilibrium. This is due to the abundant adsorption sites on the surface of BC in the

initial stage and the high Cd^{2+} content in the solution, which leads to a higher adsorption rate. In the later stage, the adsorption sites on the surface of BC tend to be saturated. The Cd^{2+} content in the solution decreases, the Cd^{2+} diffuses into the void of BC, and the adsorption rate decreases.

To deeply analyze the adsorption mechanism of coconut shell BC, peanut shell BC, and magnesium-modified BC for Cd^{2+} and the possible control steps, pseudo-first-order, pseudo-second-order kinetic, and intra-particle diffusion models were used to fit the parameters and curves, respectively, as shown in Tables 2, 3 and Fig. 5 and 6. By comparing the fitting coefficients (R^2) of the three kinetic equations in Tables 2 and 3, it was observed that the pseudo-second-order kinetic equation presents the most suitable fit. This result reflects more accurately the adsorption process of Cd^{2+} for all carbon materials. The pseudo-first- order kinetic model can adapt to the initial stage of the adsorption process, and then deviate from the adsorption process. The kinetic adsorption process of the unmodified and magnesium-modified materials was in good agreement with the pseudo-second-order kinetic model. The pseudo-first-order equation and the intra-particle diffusion model of the MgBC adsorption of Cd^{2+} presented smaller coefficient of determination values.

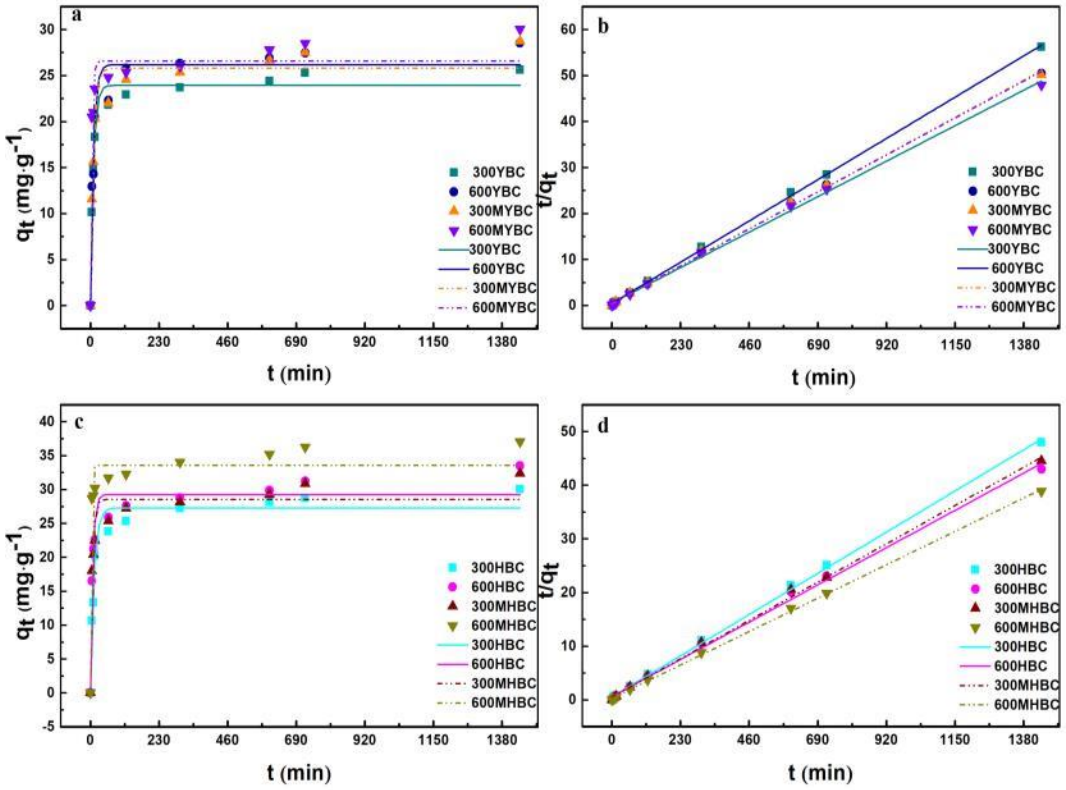

Fig. 5. Fitting parameters of the kinetic equation of Cd^{2+} with different adsorbents: (a) pseudo-first-order kinetics YBC and MYBC; (b) pseudo-second-order kinetics of YBC and MYBC; (c) pseudo-first-order kinetics of HBC and MBC and (d) pseudo-second-order kinetics of HBC and MBC

As shown in Fig. 6, the adsorption process is divided into two linear stages. The first stage represents the instantaneous adsorption, mainly surface adsorption, and the second stage represents the gentle adsorption, which indicates that the intra-particle diffusion is the main speed-limiting step. There was no linear relationship between the

amount of Cd^{2+} adsorbed by MgBC and $t^{1/2}$. Because the curve does not go through the origin, the adsorption of Cd^{2+} by coconut shell BC and peanut shell BC was controlled by intergranular diffusion and multi-step control. In addition, the adsorptive capacity of Cd^{2+} by peanut shell BC and modified peanut shell BC was greater than that of coconut shell BC and coconut shell modified BC.

Table 2. Fitting Parameters of the Kinetic Equation of Cd^{2+} with Different Adsorbents

Sample	First-order			Second-order		
	q_e (mg•g^{-1})	k_1 (h^{-1})	R^2	q_e (mg•g^{-1})	k_2 (g•mg^{-1}h^{-1})	R^2
300 YBC	24.0	0.10	0.9798	0.43	0.04	0.9995
600 YBC	26.2	0.10	0.9471	0.46	0.04	0.9992
300 MYBC	25.8	0.10	0.9524	0.58	0.03	0.9986
600 MYBC	26.6	0.23	0.9302	0.51	0.03	0.9981
300 HBC	27.3	0.08	0.9584	0.54	0.03	0.999
600 HBC	29.3	0.13	0.9351	0.59	0.03	0.9968
300 MHBC	28.6	0.14	0.9246	0.52	0.03	0.9978
600 MHBC	33.6	0.33	0.9457	0.27	0.03	0.9993

Table 3. Fitting Parameters of the Intra-Particle Diffusion of Cd^{2+} with Different Adsorbents

Adsorbent	Intra-particle diffusion model					
	K_{p1}	C_1	R^2	K_{p2}	C_2	R^2
300 YBC	1.44 ± 0.51	15.42 ± 2.40	0.7027	0.12 ± 0.02	21.35 ± 0.44	0.9727
600 YBC	1.21 ± 0.31	16.42 ± 1.46	0.8283	0.17 ± 0.05	22.70 ± 1.07	0.9004
300 MYBC	0.54 ± 0.09	27.64 ± 0.45	0.9121	0.20 ± 0.03	21.54 ± 0.74	0.9408
600 MYBC	1.84 ± 0.64	8.49 ± 3.05	0.7052	0.18 ± 0.01	23.31 ± 0.27	0.8929
300 HBC	1.61 ± 0.71	10.69 ± 3.39	0.5752	0.20 ± 0.03	23.05 ± 0.60	0.7114
600 HBC	1.63 ± 0.76	10.44 ± 3.59	0.5479	0.24 ± 0.02	24.47 ± 0.42	0.8896
300 MHBC	0.76 ± 0.27	19.25 ± 1.28	0.6937	0.23 ± 0.03	24.20 ± 0.78	0.9795
600 MHBC	2.23 ± 0.80	7.49 ± 3.78	0.6963	0.19 ± 0.02	30.49 ± 0.49	0.9222

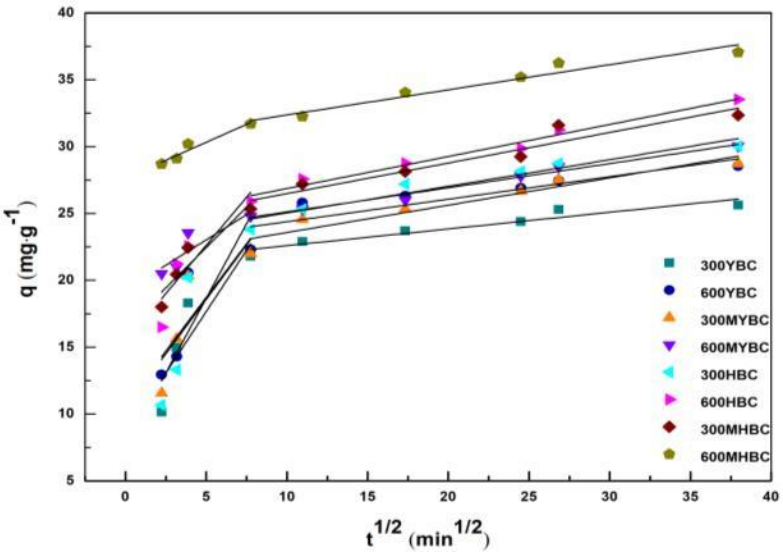

Fig. 6. Fitting curves of the intra-particle diffusion model for Cd^{2+} with different adsorbents

Adsorption isotherm

The adsorption isotherms of different adsorbents for Cd^{2+} at different temperatures are shown in Figs. 7 and 8.

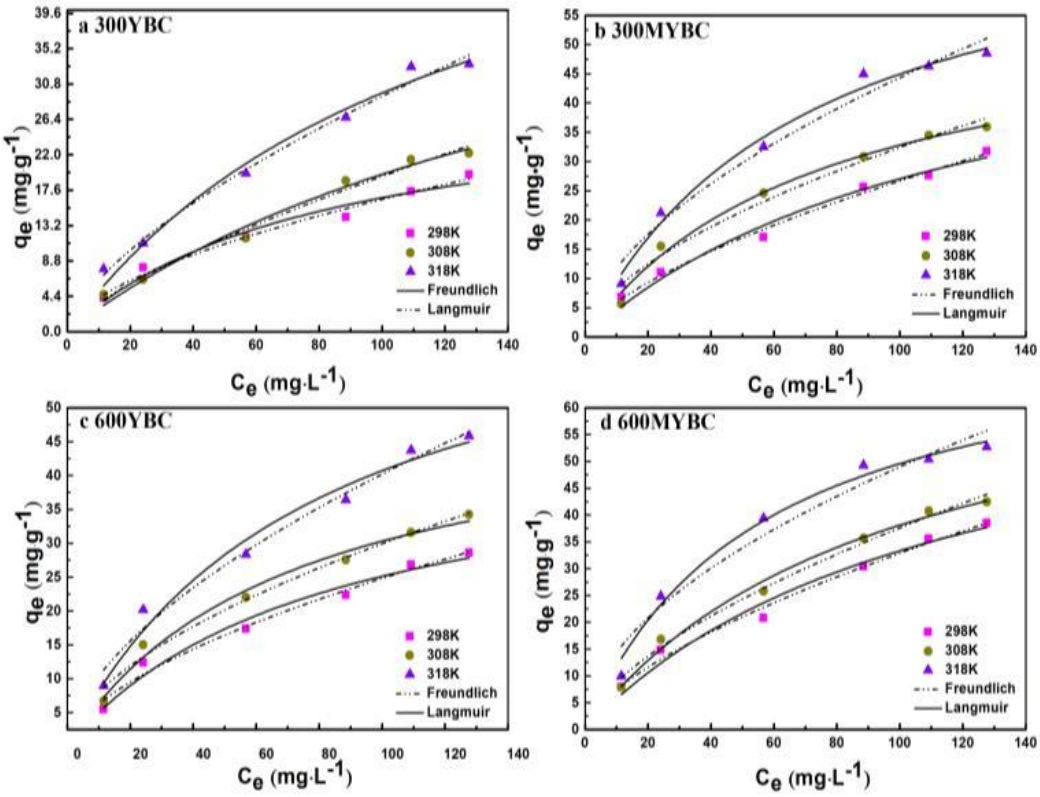

Fig. 7. Isothermal fitting curves of YBC and MYBC for Cd^{2+} at different temperatures

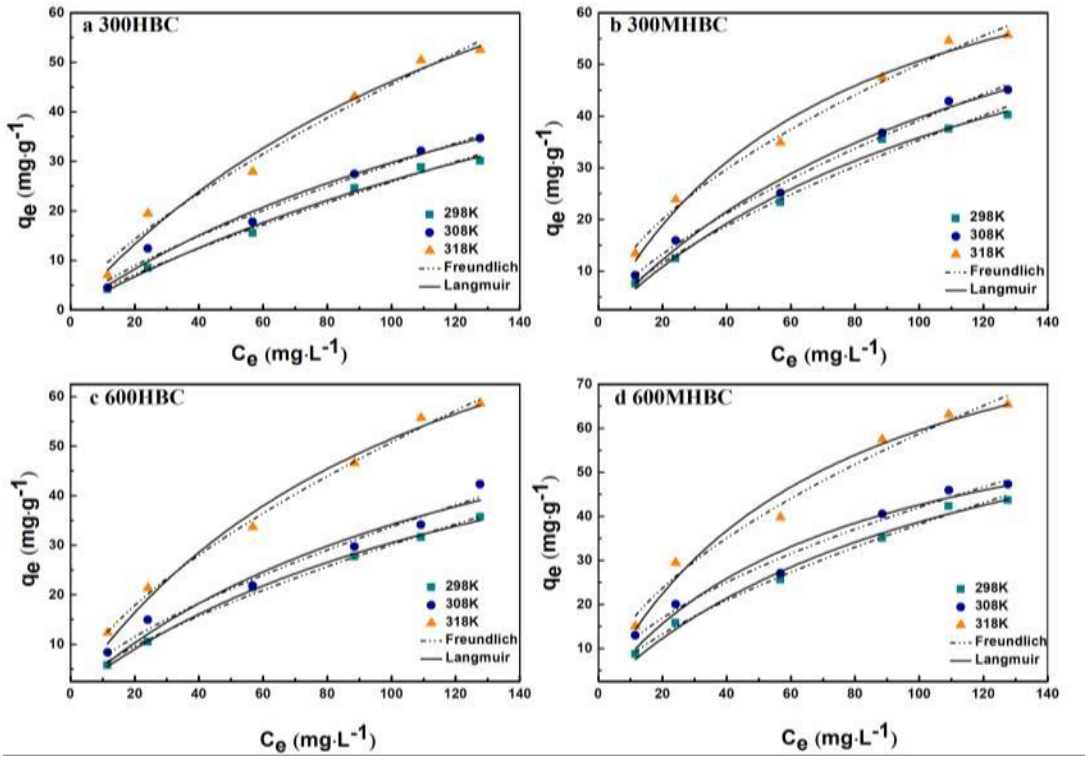

Fig. 8. Isothermal fitting curves of Cd^{2+} between HBC and MHBC at different temperatures

The Langmuir and Freundlich isotherm adsorption models were used to fit the experimental data. The fitting parameters of the isotherm adsorption model are shown in Table 4. When the initial concentration of Cd^{2+} was below 80 mg·L^{-1}, the adsorption capacity of Cd^{2+} by BC increased with the increase in Cd^{2+} concentration and reached equilibrium when the concentration was greater than 100 mg·L^{-1}. This result indicates that increasing the initial concentration of Cd^{2+} is beneficial to the adsorption of Cd^{2+} by BC. Moreover, a higher pyrolysis temperature resulted in a larger adsorption capacity. The same pyrolysis temperature promotes the adsorption of Cd^{2+} by BCs. The maximum adsorption capacity of the modified carbon material was greater than that of original carbon.

The MgO crystal formed on the modified carbon surface, which enhances the adsorption capacity of the modified carbon material. It was stronger than the original carbon material, especially 600 MHBC. The maximum adsorption capacity of the modified carbon material reached 75.35 mg·g^{-1}, which indicates that the MgO crystal formed on the modified carbon surface enhanced the adsorption capacity of the modified carbon material. MHBC had a strong adsorption capacity for cadmium-contaminated solution. Comparing the fitting coefficients R^2 of the two models, the fitting parameters R^2 of the Langmuir model were larger than that of the Freundlich model, which indicates that the Langmuir model can better describe the adsorption behavior of adsorbents of Cd^{2+}, and that they adsorb Cd^{2+} on a single layer. In addition, isothermal adsorption experiments were performed at 298 K, 308 K, and 318 K. Table 4 shows that the K_F values of the adsorbents increased with increasing ambient temperature. In particular, the adsorptive strength of adsorbents increased with the increasing ambient temperature. The Langmuir model parameters, q_m, of the adsorbents also showed an increasing trend with the increase in ambient temperature. Thus, the increase in temperature improved the

adsorptive capacity of the adsorbents for Cd^{2+}.

The environmental temperature also affects adsorption. Thermodynamic adsorption experiments were performed at 298 K, 308 K, and 318 K. The experiment was recorded at the initial Cd^{2+} concentrations of 20.0, 40.0, 80.0, 120.0, 160.0, and 200.0 $mg \cdot L^{-1}$ at 25, 35, and 45 °C. 0.05 g of the prepared samples were added to a Cd^{2+} solution and stirred at 200 rpm then filtered through a 0.45-μm filter, and analyzed by AAS. The dosage of the samples was 25 mL, and the solution pH was 6.03. To examine the adsorption thermodynamics of Cd^{2+} by MgBC, the ΔG^0 of the adsorption process was calculated by Eq. 6. The slope and intercept of T were obtained by fitting the relationship between ΔG^0 and ΔH^0 and ΔS^0, expressed in Eq. 7,

$$\Delta G^0 = -RT\ln K_0 \quad (6)$$

$$\Delta G^0 = \Delta H^0 - T\Delta S^0 \quad (7)$$

where ΔG^0 is the free energy change, ($kJ \cdot mol^{-1}$); ΔS^0 is the entropy change, ($kJ \cdot mol^{-1} \cdot K^{-1}$); ΔH^0 is the enthalpy change, ($kJ \cdot mol^{-1}$); R is the gas constant, (8.314 $J \cdot mol^{-1}.K^{-1}$); T is the thermodynamic temperature, (K); and K_0 is the Langmuir isothermal equation constant K_L multiplied by 1000; and transformed into a dimensionless number (Zhang *et al*. 2012b). The values of ΔH^0 and ΔS^0 are shown in Table 5.

Table 4. Isothermal Adsorption Model Parameters of Cd^{2+} by Different Adsorbents Adsorption Thermodynamics

Adsorbent	Temperature (K)	Freundlich			Langmuir		
		K_F	*n*	R^2	q_m	K_L	R^2
300 YBC	298	1.08 ± 0.23	0.5913 ± 0.0470	0.9780	66.04 ± 11.81	0.0082 ± 0.0026	0.9827
	308	0.66 ± 0.20	0.7320 ± 0.0652	0.9612	30.30±4.90	0.0122 ± 0.0041	0.9814
	318	1.41 ± 0.30	0.6587 ± 0.0463	0.9780	55.99 ± 15.20	0.0054 ± 0.0022	0.9874
600 YBC	298	1.59 ± 0.37	0.5966 ± 0.0508	0.9724	45.65 ± 6.32	0.0122 ± 0.0035	0.9807
	308	2.13 ± 0.44	0.5731 ± 0.0457	0.9829	51.76 ± 4.86	0.0141 ± 0.0029	0.9835
	318	2.66 ± 0.62	0.5893 ± 0.0516	0.9796	72.60 ± 9.46	0.0128 ± 0.0035	0.9736
300 MYBC	298	1.30 ± 0.24	0.6555 ± 0.0401	0.9752	60.04 ± 11.27	0.0082 ± 0.0027	0.9903
	308	2.11 ± 0.65	0.5931 ± 0.0682	0.9879	57.55 ± 5.07	0.0133 ± 0.0025	0.9668
	318	3.14 ± 0.97	0.5751 ± 0.0683	0.9855	76.61 ± 6.88	0.0142 ± 0.0028	0.9638
600 MYBC	298	1.67 ± 0.35	0.6475 ± 0.0454	0.9702	72.04 ± 14.17	0.0086 ± 0.0030	0.9873
	308	2.08 ± 0.40	0.6284 ± 0.0428	0.9882	74.80 ± 7.50	0.0104 ± 0.0020	0.9895
	318	4.23 ± 1.50	0.5317 ± 0.0786	0.9431	77.26 ± 5.98	0.0179 ± 0.0034	0.9839
300 HBC	298	0.65 ± 0.17	0.8024 ± 0.0627	0.9891	94.78 ± 23.48	0.0038 ± 0.0013	0.9926
	308	0.97 ± 0.30	0.7416 ± 0.0668	0.9787	85.51± 23.42	0.0053 ± 0.0022	0.9816
	318	1.64 ± 0.54	0.7218 ± 0.0724	0.9767	121.10 ±30.39	0.0062 ± 0.0025	0.9770
600 HBC	298	1.14 ± 0.16	0.7108 ± 0.0316	0.9479	75.76 ± 5.57	0.0067 ± 8.1197	0.9976
	308	1.55 ± 0.48	0.6692 ± 0.0676	0.9471	81.59 ± 25.15	0.0072±0.0037	0.9738
	318	2.55 ± 0.36	0.6500 ± 0.0309	0.9942	110.72 ± 16.25	0.0087 ± 0.0023	0.9833
300 MHBC	298	1.45 ± 0.39	0.6929 ± 0.0581	0.9372	1.45 ± 0.39	0.6929 ± 0.0581	0.9834
	308	1.79 ± 0.31	0.6704 ± 0.0375	0.9922	1.79 ± 0.31	0.6704 ± 0.0375	0.9922
	318	3.65 ± 0.61	0.5684 ± 0.0369	0.9883	3.65 ± 0.61	0.5683 ± 0.0369	0.9884
600 MHBC	298	1.85 ± 0.30	0.6576 ± 0.0356	0.9900	84.07±11.31	0.0085 ± 0.0021	0.9940
	308	3.09 ± 0.72	0.5671 ± 0.0516	0.9504	75.01 ± 12.55	0.0132 ± 0.0047	0.9766
	318	4.37 ± 1.00	0.5643 ± 0.0506	0.9780	101.42 ± 12.15	0.0142 ± 0.0037	0.9722

Based on the experimental data of the adsorbent adsorbing Cd^{2+} at 298 K, 308 K, and 318 K, a thermodynamic analysis of adsorption was performed. The thermodynamic analysis diagrams are shown in Figs. 5 and 6, and the thermodynamic parameters are shown in Table 5. Table 5 demonstrates that the Gibbs free energy of different adsorbents was negative, indicating that adsorbents adsorbed Cd^{2+} spontaneously. Moreover, ΔG^0 decreased with the increase of temperature, indicating that the increase of ambient temperature plays a positive role in spontaneous adsorption. The enthalpy change ΔH^0 was positive, indicating that the adsorbent adsorbing Cd^{2+} is an endothermic process at 298 to 318 K. The entropy change ΔS^0 was positive, indicating that the adsorbent adsorbs Cd^{2+} spontaneously. The structure of the adsorbents and heavy metals changes during the adsorption process. The entropy changed to a positive value of ΔS^0, which suggests that the order of the adsorbate molecules decreases, and the degree of chaos increased during the adsorption process (Lang *et al*. 2015).

Table 5. Thermodynamic Model Parameters of Adsorption of Cd^{2+} by Different Adsorbents

Adsorbent	ΔG^0/(KJ·mol^{-1})			ΔH^0/ (KJ·mol^{-1})	ΔS^0/ (KJ·mol^{-1}·K^{-1})	R^2
	298 K	308 K	318 K			
300 YBC	-5.21314	-6.4055	-7.4586	28.2230	0.11227	0.9974
600 YBC	-6.19749	-6.7761	-6.740356	1.7889	0.02714	0.4017
300 MYBC	-5.21314	-6.6265	-7.014779	21.4604	0.09008	0.4017
600 MYBC	-5.33115	-5.9967	-7.626986	29.0377	0.11479	0.8888
300 HBC	-3.30756	-4.2705	-4.823838	19.2167	0.07581	0.9525
600 HBC	-4.71261	-5.0551	-5.719506	10.3438	0.05034	0.9341
300 MHBC	-16.2055	-16.665	-16.76903	7.8684	0.02818	0.7663
600 MHBC	-5.30217	-6.6072	-7.014779	20.0662	0.08563	0.8323

Effect of pH

The adsorption of Cd^{2+} in aqueous solution in different initial pH conditions is shown in Fig. 9. The initial pH of the solution had a great influence on the adsorption of Cd^{2+} and showed a trend of rapid growth and then slow growth. The adsorption of Cd^{2+} by BC in Figs. 9a and 9b increased with the increased solution pH. In Fig. 9a, when the pH was 3 to 7, the adsorption capacity increased rapidly, and when the pH was greater than or equal to 7, the adsorption capacity increased slowly. In Fig. 9b, when the pH was 3 to 6, the adsorption capacity increased rapidly, and when the pH was greater than or equal to 6, the adsorption capacity increased slowly.

The adsorption amount varied with the initial value of the solution because, at low pH, the adsorption sites on the surface of the carbon particles were occupied by a large number of H^+, which prevented the approach of Cd^{2+}. Therefore, the removal rate of Cd^{2+} was relatively low. With increasing pH, the negative charge on the surface of carbon increases (Houben *et al*. 2013), and the electrostatic attraction of Cd^{2+} increases. With the increase in pH, the surface of biomass carbon is negatively charged.

Biomass carbon mainly depends on the electrostatic adsorption of heavy metal ions in solution (Kadirvelu and Namasivayam 2004). In addition, because of the electronic layer structure of Cd^{2+}, the increase in pH stimulates hydrolysis, and the adsorption affinity of BC by metal hydroxyl ions produced by the hydrolysis is greater than that of free ions (Fristak *et al*. 2015).

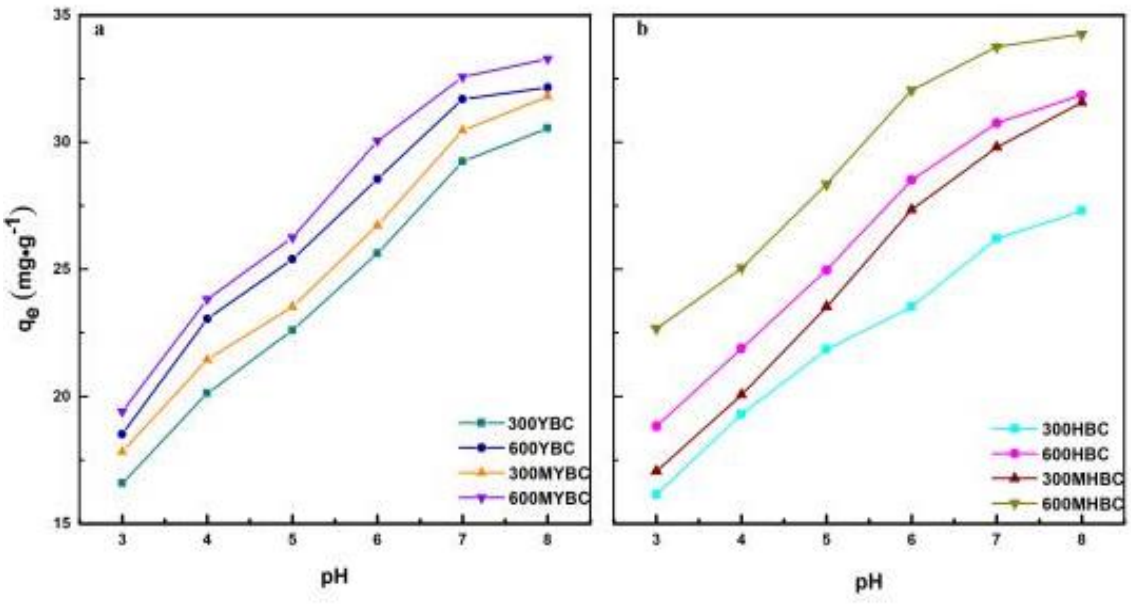

Fig. 9. Adsorption of Cd^{2+} in an aqueous solution under different initial pH conditions: (a) YBC and MYBC and (b) HBC and MHBC

CONCLUSIONS

1. Coconut and peanut shells were used as raw materials. Magnesium oxide was formed on the surface of coconut and peanut shell BC by using a chemical impregnation method. Magnesium-loaded BC materials were prepared, which had good adsorption effect on Cd^{2+}.
2. The results of SEM-EDS, BET, and FTIR analyses showed that MgO was successfully loaded on BC and played an important role in the adsorption of Cd^{2+}.
3. The pseudo-second-order kinetics and Langmuir isothermal adsorption equation accurately described the adsorption process of BC and MBC for Cd^{2+}. At a higher temperature, the adsorptive performance of adsorbents was better. At high pH, the adsorptive effect of the modified material for Cd^{2+} was stronger. At the same time, under the same adsorption conditions, the amount of Cd^{2+} adsorbed by peanut shell BC and modified peanut shell BC was larger than that by coconut shell BC and modified coconut shell BC.
4. The MgO particles on the surface of the modified material play an important role in the adsorption of Cd^{2+}, and the adsorption process mainly consists of chemical adsorption. MBC is a low-cost adsorbent that has strong adsorptive properties on Cd^{2+} and a great potential for environmental remediation.

ACKNOWLEDGMENTS

This study was supported by the National Natural Science Foundation of China (No. 41501542).

REFERENCES CITED

Ahmad, M., Rajapaksha, A. U., Lin, E, J., and Yong, O, S. (2013). "Biochar as a sorbent for contaminant management in soil and water: A review." *Chemosphere* 99(3): 19-33.

Beesley, L., Moreno-Jiménez, E., Gomez-Eyles, J. L., Harris, E., Robinson, B., and Sizmur, T. (2011). "A review of biochars potential role in the remediation, revegetation and restoration of contaminated soils," *Environmental Pollution* 159, 3269-3282.

Chen, Q., Qin, J., Sun, P., Cheng, Z., and Shen, G. (2018). "Cow dung-derived engineered biochar for reclaiming phosphate from aqueous solution and its validation as slow-release fertilizer in soil crop system," *Journal of Cleaner Production* 172, 2009-2018. DOI: 10.1016/j.jclepro.2017.11.224

Cui, D, D., Jiang, J, C., Sun, K., and Lu, X, C. (2010). "Preparation and properties of bamboo-based activated carbon with high specific surface area," *Chemistry and Industry of Forest Products* 30(5), 57-60. · ·

Fang, C., Zhang, T., Li, P., Jiang, R., Wu, S., Nie, H., and Wang, Y. (2015). "Phosphorus recovery from biogas fermentation liquid by Ca-Mg loaded biochar," *Journal of Environmental Sciences* 29, 106-114. DOI: 10.1016/j.jes.2014.08.019

Fang, C., Zhang, T., Li, P., Jiang, R.-f., and Wang, Y.-c. (2014). "Application of magnesium modified corn biochar for phosphorus removal and recovery from swine wastewater," *International Journal of Environmental Research and Public Health* 11(9), 9217-9237. DOI: 10.3390/ijerph110909217

Feng, Z., Chen, N., Feng, C., and Gao, Y. (2018). "Mechanisms of Cr(VI) removal by $FeCl_3$- modified lotus stem-based biochar ($FeCl_3$@ LS-BC) using mass-balance and functional group expressions," *Colloids and Surfaces a-Physicochemical and Engineering Aspects* 551, 17-24. DOI: 10.1016/j.colsurfa.2018.04.054

Frišták, V., Pipíška, M., Lesný, J., Soja, G., Friesl-Hanl, W., and Packová, A. (2015). "Utilization of biochar sorbents for Cd^{2+}, Zn^{2+}, and Cu^{2+} ions separation from aqueous solutions: comparative study," *Environmental Monitoring & Assessment* 187(1), 1-16.

Houben, D., Evrard, L., and Sonnet, P. (2013). "Mobility, bioavailability and ph-dependent leaching of cadmium, zinc and lead in a contaminated soil amended with Biochar," *Chemosphere* 92(11), 1450-1457.

Inyang, M., Gao, B., Pollammanappallil, P., and Ding, W, C., and Zimmerman, A, R. (2010). "Biochar from anaerobically digested sugarcane bagasse," *Bioresource technology* 101(22):8868-8872.

Jia, Z., Deng, J., Chen, N., Shi, W., Tang, X., and Xu, H. (2016). "Bioremediation of cadmium-dichlorophen co-contaminated soil by spent *Lentinus edodes* substrate and its effects on microbial activity and biochemical properties of soil," *Journal of Soils and Sediments* 17(2), 1-11. DOI: 10.1007/s11368-016-1562-7

Jian, M. F., Gao, K. f., and Yu, H. P. (2016). "Effects of different pyrolysis temperatures on the preparation and characteristics of bio-char from rice straw," *Acta Scientiae Circumstantiae* 36(05), 1757-1765.

Ju, H., Kim, K., Park, D., and Kim, J. (2018). "Fabrication of porous SnSeS nanosheets with controlled porosity and their enhanced thermoelectric performance," *Chemical Engineering Journal* 335, 560-566. DOI: 10.1016/j.cej.2017.11.003

Jung, K.-W., Jeong, T.-U., Hwang, M.-J., Kim, K., and Ahn, K.-H. (2015b). "Phosphate

adsorption ability of biochar/Mg-Al assembled nanocomposites prepared by aluminum-electrode based electro-assisted modification method with $MgCl_2$ as electrolyte," *Bioresource Technology*198, 603-610.DOI: 10.1016/j.biortech. 2015.09.068

Jung, K.-W., and Ahn, K.-H. (2016). "Fabrication of porosity-enhanced MgO/BC for removal of phosphate from aqueous solution: Application of a novel combined electrochemical modification method," *Bioresource Technology* 200, 1029-1032. DOI: 10.1016/j.biortech.2015.10.008

Kadirvelu, K., and Namasivayam, C. (2004). "Erratum to "Activated carbon from coconut coirpith as metal adsorbent: adsorption of cd(ii) from aqueous solution," *Advances in Environmental Research* 7(2), 471-478.

Lang, Y, H., Wang, H., and Liu W. (2015). "Effect of pomelo peel biochars on adsorption performance of phosphorus in soil," *Periodical of Ocean University of China* 45(04),78-84 DOI: 10.16441/j.cnki.hdxb.20140100

Liu, H., Wu, S, H., Sun, Y., and Xu, R., Qiu, P, H., Li, K, F., and Qin, Y, K. (2005). "Specific area and pore structure of lignite char under the condition of fast pyrolysis," *Proceedings of the CSEE* (12), 86-90. DOI: 10.13334/j.0258-8013.pcsee.2005.12.016

Liu, H., Xu, F., Xie, Y., Wang, C., Zhang, A., Li, L., and Xu, H. (2018a). "Effect of modified coconut shell biochar on availability of heavy metals and biochemical characteristics of soil in multiple heavy metals contaminated soil," *Science of the Total Environment* 645, 702-709. DOI: 10.1016/j.scitotenv.2018.07.115

Luo, C. (2018). "Discussion on remediation technology of soil cadmium pollution," *China Resources Comprehensive Utilization* 375(02), 79-81+89.

Marco, K., Nico, P, S., and Johnson, M, G. (2010). "Dynamic molecular structure of plant biomass-derived black carbon (BC)," *Environmental Science and Technology* 44 (4), 1247-1253

Meng, Q, R., Cui, X., H., Zhu, Y., and He, X. (2017). "Characterization of MgO-loaded aquatic plants biochar and its adsorption capacity of phosphorus in aqueous solution," *Acta Scientiae Circumstantiae* 37(8), 2960-2967. DOI: 10.13671/j.hjkxxb.2017.0075

Novais, S. V., Oliveira Zenero, M. D., Tronto, J., Conz, R. F., and Pellegrino Cerri, C. E. (2018). "Poultry manure and sugarcane straw biochars modified with $MgCl_2$ for phosphorus adsorption," *Journal of Environmental Management* 214, 36-44. DOI: 10.1016/j.jenvman.2018.02.088

Paranavithana, G. N., Kawamoto, K., Inoue, Y., Saito, T., Vithanage, M., Kalpage, C. S., and Herath, G. B. B. (2016). "Adsorption of Cd^{2+} and Pb^{2+} onto coconut shell biochar and BC-mixed soil," *Environmental Earth Sciences* 75(6). DOI: 10.1007/s12665-015-5167-z

Rajapaksha, A, U., Chen, S, S., Tsang, D, W., Zhang, M., Vithanage, M., Mandal, S., and Ok, Y, S. (2016). "Engineered/designer biochar for contaminant removal /immobilization from soil and water: Potential and implication of biochar modification," *Chemosphere* 148, 276-291. DOI: 10.1016 /j. chemosphere. 2016.01.043

Song, Z., Lian, F., Yu, Z., Zhu, L., Xing, B., and Qiu, W. (2014). "Synthesis and characterization of a novel MnOx-loaded biochar and its adsorption properties for Cu^{2+} in aqueous solution," *Chemical Engineering Journal* 242, 36-42. DOI: 10.1016/j.cej.2013.12.061

Sun, X., Shan, R., Li, X., Pan, J., Liu, X., Deng, R., and Song, J. (2017). "Characterization of 60 types of Chinese biomass waste and resultant biochars in

terms of their candidacy for soil application," *Global Change Biology Bioenergy* 9, 1423-1435. DOI:10.1111/gcbb.12435.

Takaya, C. A., Fletcher, L, A., and Singh, S. (2016). "Recovery of phosphate with chemically modified biochars," *Journal of Environmental Chemical Engineering* 4, 1156-1165.

Tang, W. W., Zeng, G. M., Gong, J. L., Liang, J., Xu, P., Zhang, C., and Huang, B. B. (2014). "Impact of humic/fulvic acid on the removal of heavy metals from aqueous solutions using nanomaterials: A review," *Science of the Total Environment* 468, 1014-1027. DOI: 10.101 6/j.scitotenv.2013.09.044

Wang, S., Gao, B., Li, Y., and Mosa, A., Zimmerman, A. R., Ma, L. Q., and Migliaccio, K. W. (2015). "Manganese oxide-modified biochars: Preparation, characterization, and sorption of arsenate and lead," *Bioresource Technology* 181, 13-17. DOI: 10.1016/j.biortech.2015.01.044

Xu, Y, L., Cheng, f., Chen, G, J., and Zhong, J, A., Yang, W., and Xue, L, H., (2015). "Fractal characteristics of shale pores of Longmaxi Formation In southeast Sichuan Basin," *Lithologic Reservoirs* 27(04), 32-39.

Yang, X., Zhang, S, Q., Hou, Q, D., and Wang, Y, N., Ju, M, T., Liu, L. (2018). "The preparation of biochar and adsorption behavior of Mg-modified biochar to pollutants,"*Acta Scientiae Circumstantiae* 38(10), 4032-4043.

Yao, Y., Gao, B., Chen, J., and Yang, L. (2013). "Engineered biochar reclaiming phosphate from aqueous solutions: Mechanisms and potential application as a slow-release fertilizer," *Environmental Science & Technology* 47(15), 8700-8708. DOI: 10.1021 /es4012977

Yuan, J, H., Xu, R, K., and Zhang, H. (2011). "The forms of alkalis in the biochar produced from crop residues at different temperatures," *Bioresource Technology* 102(3), 3488-3497. DOI: 10.1016/j.biortech.2010.11.018

Zhang, M., Gao, B., Varnoosfaderani, S., Hebard, A., Yao, Y., and Inyang, M. (2013). "Preparation and characterization of a novel magnetic biochar for arsenic removal," *Bioresource Technology* 130, 457-462. DOI: 10.1016/j.biortech.2012.11.132

Zhang, S, Z., Wu, L, W., and Cheng, Z, M. (2012b). "Study on point of zero charge and adsorption of the diatomite," *Journal of Chongqing University of Technology* 2012, 26(2), 36-39.

Zhou, Q., Liao, B., Lin, L., Qiu, W., and Song, Z. (2018). "Adsorption of Cu(II) and Cd(II) from aqueous solutions by ferromanganese binary oxide-biochar composites," *Science of the Total Environment* 615, 115-122. DOI: 10.1016 /j. scitotenv. 2017. 09.220

Article submitted: July 26, 2019; Peer review completed: October 10, 2019; Revised version received: November 19, 2019; Accepted: November 22, 2019; Published: December 11, 2019.
DOI: 10.15376/biores.15.1.767-786

APPENDIX

Supplementary Material

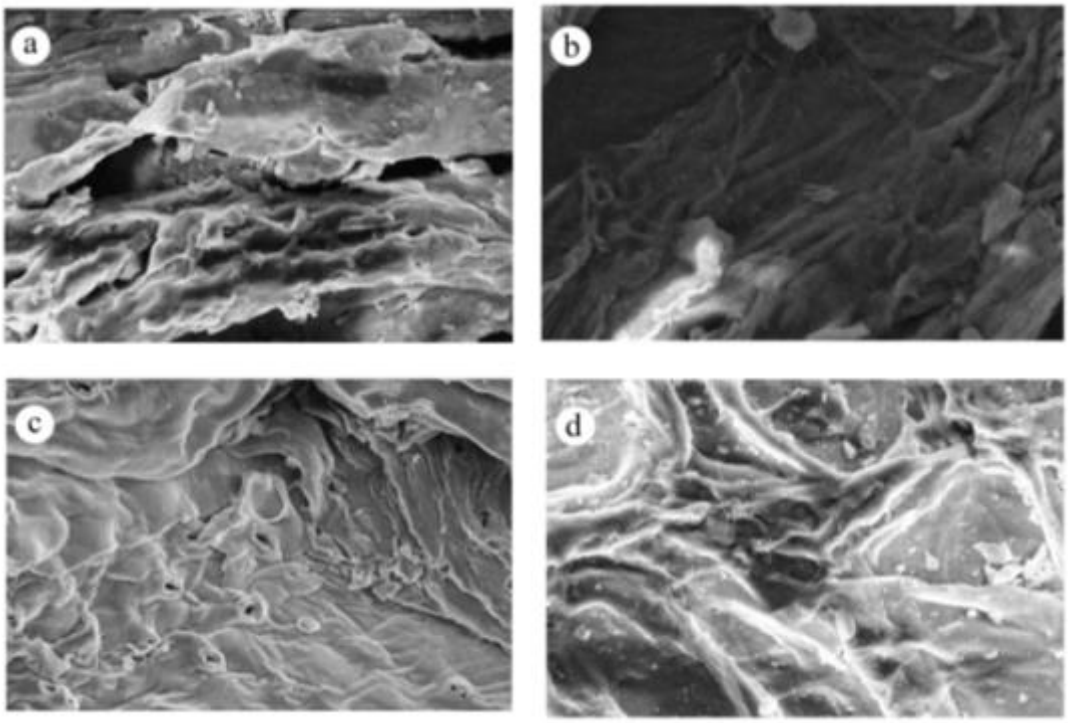

Fig. S1. SEM diagrams of YBC and MYBC at different temperatures: (a) 300 YBC, (b) 600 YBC, (c) 300 MYBC; and (d) 600 MYBC

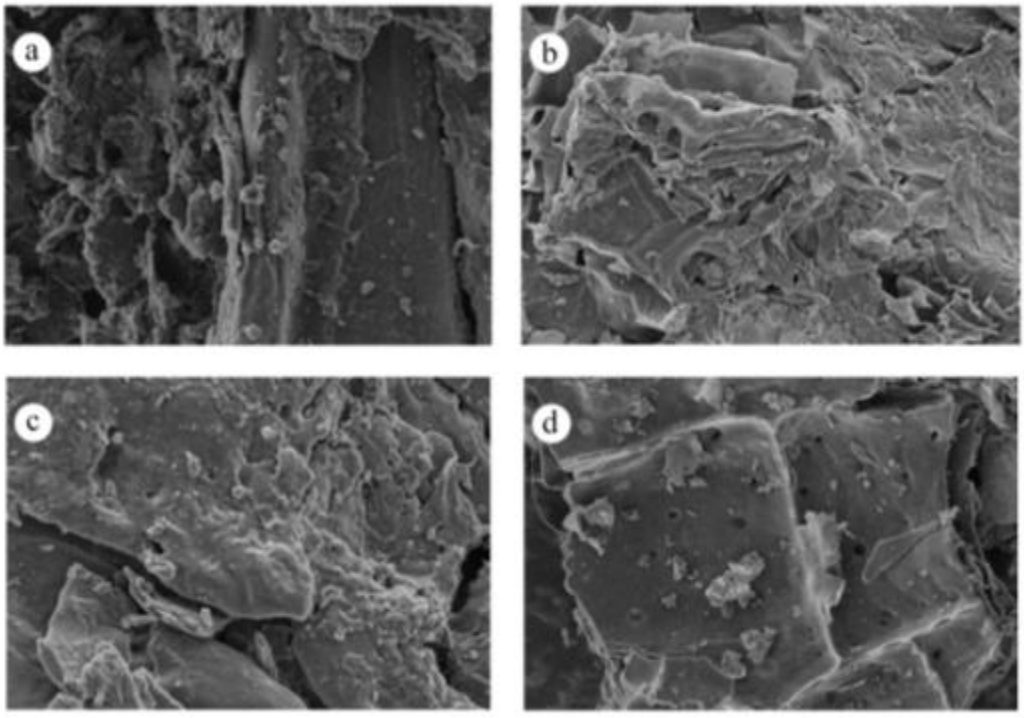

Fig. S2. SEM diagrams of HBC and MHBC at different temperatures: (a) 300 HBC, (b) 600 HBC, (c) 300 MHBC; and (d) 600 MHBC